

Polarized light emission from graphene induced by terahertz pulses

*I. V. Oladyshkin, S. B. Bodrov, A. V. Korzhimanov, A. A. Murzanev, Yu. A. Sergeev, A. I. Korytin,
M. D. Tokman and A. N. Stepanov*

Institute of Applied Physics of the Russian Academy of Sciences, 603950, Nizhny Novgorod, Russia

Polarized spontaneous optical emission from graphene irradiated by intense single-cycle terahertz (THz) pulses was investigated experimentally and explained theoretically. We found that emitted photons are polarized predominantly perpendicular to the THz electric field, which proves that the THz-field-induced optical emission is a non-thermal physical effect. Comparison of the measured optical spectrum and polarization anisotropy with the results of numerical modeling allowed us to estimate a momentum isotropization time for electrons in graphene to be ~ 35 fs and roughly reconstruct the distribution function evolution in k -space.

Graphene is one of perspective materials attracting attention due to unusual properties of charge carriers and unique characteristics like 2D geometry, high nonlinearity, record electrical and thermal conductivity etc. Nonlinear and quantum optics of graphene is now actively investigated [1-14]. Over the past few years, ultrafast kinetics of electrons in graphene became one of the central topics in a large number of fundamental and applied studies of various subpicosecond processes. In particular, it was found that femto- and picosecond relaxation processes play a key role in the effects like nonlinear THz response [7, 8, 15], surface plasmon generation [10, 11, 16, 17], nonlinear transmission [8, 12], high harmonic generation [18-24], inverse Faraday effect, generation of edge photocurrents [9, 25] and many others.

At the same time, dynamics of elementary relaxation processes at ultrashort timescales in graphene and other materials is still a relevant problem due to limitations of available experimental techniques and high complexity of first-principle modeling. Here we should mention recent attempt to control and measure e - e electron scattering length in graphene in a state-of-art experiment [26]. To date, various pump-probe experiments (THz pump – optical probe [27], optical pump – THz probe [28], optical pump – optical probe [29-31]) and theoretical works [32–35] were devoted to the investigation of ultrafast carrier dynamics in graphene, especially the thermalization and recombination processes. In particular, it was demonstrated that the characteristic time of interband recombination (~ 1 ps) significantly exceeds the times of carrier thermalization and cooling (100–300 fs).

Recently, in [37] THz-induced spontaneous optical emission of graphene in the range of 350–600 nm was observed (at peak THz electric fields from 100 to 250 kV/cm). To explain the experimental results an analytical theory based on electron-hole pair production by *Schwinger-like* (or *Landau-Zener*) transitions in strong electric field was proposed. The thermal mechanism which can also contribute to the optical emission was estimated to be two orders weaker than the measured one. At the same time, in [27] the dominant role of impact ionization, or interband reverse Auger recombination, in the process of electron-hole pair production by strong THz field was stated¹.

¹ Interband reverse Auger recombination is forbidden in ideal 2D Dirac systems due to the energy and momentum conservation laws [38–40]. In general case the efficiency of interband Auger processes is determined by the lattice imperfection (e.g. trigonal warping [41]) or by the distortion of conservation laws for two-particle collisions (which was a fitting parameter in [27]) in the presence of an additional interaction – with phonons [39, 40] or others.

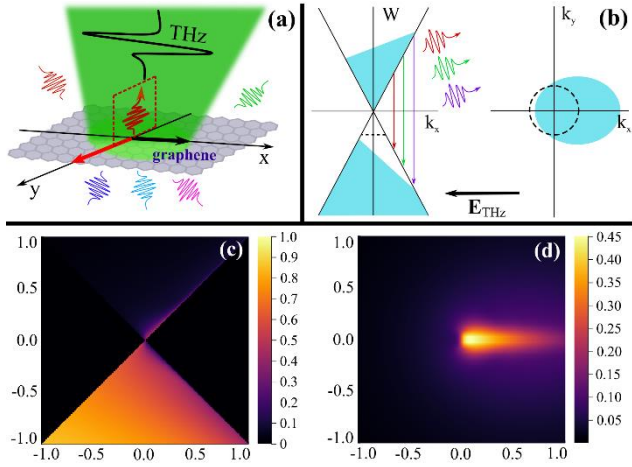


Fig. 1. (a) Geometry of the problem. (b) A sketch of the electron distribution function evolution. Initial Fermi level is shown by dashed line, interband transitions are shown by color arrows. (c) Numerically calculated distribution of electrons over two bands at the moment of 300 kV/cm THz pulse action. (d) The same moment in k -space of the conduction band (k_x , k_y). Color bars represent occupation probability, unit scale of vertical and horizontal axis corresponds to $\hbar k v_F = 1$ eV.

In this Letter we provide more clear experimental evidences of strongly non-thermal character of THz-field-induced optical emission from graphene basing, first of all, on polarization measurements. For this we investigate spectral and polarization properties of the optical emission in the spectral range of 350-1050 nm. In combination with the numerical modeling and analytical estimations, this allows us to estimate the temperature of electrons at different magnitudes of pumping THz field and to roughly reconstruct a typical distribution function in k -space, which occurred to be significantly anisotropic.

Let us start with a theoretical model of graphene excitation. In [37] the basic analytical model describing the electron-hole pair production and spontaneous optical emission of graphene in THz field was developed. In contrast to [37], here we do not use the assumption of instantaneous isotropization and model dynamics of the electronic distribution function in k -space including both the isotropization and recombination stages. Figure 1(a) illustrates the geometry of the problem. Terahertz pulse polarized along the x -axis with the electric field $E_x(t)$ incidents normally on a monolayer graphene. Under the action of strong THz field, the intense electron-hole pair production starts and the anisotropic distribution function is formed both in the lower and upper bands (see Fig. 1(b)). To calculate the population inversion and corresponding spontaneous optical emission we use numerical model based on the density matrix equations for a two-band system in a homogeneous electric field [23] which is a version of the semiconductor Bloch equations:

$$\left(\frac{\partial}{\partial t} + i\omega_k + \gamma_a - \frac{eE_x(t)}{\hbar} \frac{\partial}{\partial k_x} \right) \rho_{\mathbf{k}} = -i \frac{\Omega_k}{2} [n_c(\mathbf{k}) - n_v(\mathbf{k})], \quad (1)$$

$$\frac{\partial n_{c,v}(\mathbf{k})}{\partial t} - \frac{e}{\hbar} E_x(t) \frac{\partial n_{c,v}(\mathbf{k})}{\partial k_x} = \mp i\Omega_k \text{Im}(\rho_{\mathbf{k}}) + R_{c,v}(\mathbf{k}), \quad (2)$$

where e is the elementary charge, $n_{c,v}(\mathbf{k})$ are the electron populations in the conduction and valence bands respectively, $\rho_{\mathbf{k}} = \rho_{cv; \mathbf{k}\mathbf{k}}$ is the interband quantum coherence, $\omega_k = 2v_F k$ is a local interband transition frequency at a given point of the k -space, v_F is the Fermi velocity ($\sim 10^8$ cm/s), $\Omega_k = \frac{e}{k\hbar} \sin\theta_k E_x$ is a local Rabi frequency, θ_k is an angle between \mathbf{k} and x -axis, γ_a^{-1} is the relaxation time for the interband quantum coherence and $R_{c,v}(\mathbf{k})$ are phenomenological operators of the populations relaxation in the conduction and valence bands respectively.

The operators of population relaxation are set in the BGK (Bhatnagar–Gross–Krook) form which is the simplest model. However, we assume an existence of two characteristic timescales: “fast” intraband relaxation (described by γ_a) and “slow” interband recombination (described by γ_r). For the sake of simplicity, the intraband relaxation constant¹ is supposed to be equal to the coherence relaxation rate γ_a :

$$R_{c,v}(\mathbf{k}) = -\gamma_a [n_{c,v}(\mathbf{k}) - n_{c,v}^F(k)] - \gamma_r [n_{c,v}(\mathbf{k}) - n_{0(c,v)}^F(k)]. \quad (3)$$

Here

$$n_{c,v}^F(k) = \frac{1}{1 + \exp[(\pm v_F \hbar k / 2 - \mu_{c,v}) / T]} \quad (4)$$

are quasiequilibrium local Fermi distributions in the conduction and valence bands with a preset temperature of electrons T and varying chemical potentials $\mu_{c,v}$. The chemical potentials $\mu_{c,v}$ are calculated independently using the following normalization relations which include the numbers of charge carriers in each band in the current moment of time:

$$\iint_{\infty} n_c(\mathbf{k}) d^2k = 2\pi \int_0^{\infty} n_c^F(k) k dk, \quad \iint_{\infty} [1 - n_v(\mathbf{k})] d^2k = 2\pi \int_0^{\infty} [1 - n_v^F(k)] k dk, \quad (5)$$

and

$$n_{0(c,v)}^F(k) = \frac{1}{1 + \exp[(\pm v_F \hbar k / 2 - \mu_0) / T]}, \quad (6)$$

which is a globally equilibrium Fermi distribution with the initial chemical potential μ_0 .

As it was demonstrated previously [37, 43, 44], the temperature of electrons in graphene tends to be saturated around the value of 0.2–0.25 eV. For single-cycle THz pulses the saturation was reached at the amplitudes of around 200–250 kV/cm [37]. Presumably, the reason is in strong heat absorption by optical phonons having an excitation threshold of about 0.2 eV. That is why this phenomenon cannot be correctly described without involving crystal lattice dynamics.

Basing on previously reported results, we suppose that in our experimental conditions we operate slightly below the region of temperature saturation. For better fitting of the experimental data, we introduced the $T(E_{THz})$ dependence in our numerical model and estimated its local slope. As for the relaxation rates, we kept the interband relaxation time γ_r^{-1} constant as its variation in the range 0.3–1 ps didn’t significantly affect the simulations. So, we put it to be equal to 500 fs. The intraband relaxation γ_a^{-1} time, at contrast, significantly alters the polarization properties of the spontaneous emission, which was used to estimate the anisotropy relaxation rate from experimental data. More details about the numerical scheme can be found in Supplementary Materials.

A typical distribution function of electrons in a strong THz field obtained in numerical modeling is shown in Fig. 1(c, d): the THz magnitude is 300 kV/cm, the full pulse duration is 500 fs, the moment of maximal electric field action is shown. The calculations predict an intense electron-hole pair production ($\sim 10^{12} - 10^{13}$ pairs per cm^2) and significant anisotropy of the electron velocities. The area with population inversion reaches the energy level of ~ 0.5 eV, which corresponds to direct interband transitions with 1.0 eV energy.

¹ The discussed phenomenological model of relaxation might, in principle, include two different characteristic timescales of intraband relaxation: the isotropization time γ_{a1}^{-1} and several times greater thermalization time γ_{a2}^{-1} instead of the universal constant γ_a^{-1} . However, the recombination time γ_r^{-1} undoubtedly exceeds both the γ_{a1}^{-1} and γ_{a2}^{-1} , so the quasiequilibrium distributions inside each band are formed faster than the totally equilibrium distribution. That is why this kind of model complication cannot significantly influence the experimental data interpretation, but, on the contrary, adds another one poorly known free parameter.

Distribution function anisotropy in the presence of intense interband transitions in strong THz field can be also estimated analytically. According to the ballistic ionization model [37], the density of electrons in the conduction band increases with the following rate¹:

$$\dot{N}_c = \left(\frac{eE_x}{\hbar}\right)^{\frac{3}{2}} \frac{(\bar{n}_v - \bar{n}_c)}{\pi^2 \sqrt{v_F}}, \quad (7)$$

where N_c is the number of electrons in the conduction band per cm^2 and $\bar{n}_{v,c}$ are averaged populations in the valence and conduction bands respectively. At the same time, in the simplest model of relaxation, the stationary shift of the distribution function along the THz field in k -space in the conduction band can be estimated as

$$\delta k_x = \frac{eE_x}{\hbar\gamma_a}. \quad (8)$$

To roughly estimate a relative deformation of the distribution function we introduce a parameter η , defined as a ratio between δk_x and the “local” Fermi wavenumber in the conduction band $k_F = \sqrt{\pi N_c}$. Estimating the number of excited electrons N_c using Eq. (7) in assumption that $\bar{n}_v \approx 1$, $\bar{n}_c \ll 1$ for the characteristic duration of the THz pulse τ_{THz} we arrive to:

$$\eta = \frac{\delta k_x}{\sqrt{\pi N_c}} = \frac{\pi}{\gamma_a} \left(\frac{eE_x v_F}{\hbar \tau_{THz}^2} \right)^{\frac{1}{4}}. \quad (9)$$

Thus, the relative deformation of the distribution function is proportional to $E_x^{1/4}$, so the dependence is rather weak. This is a consequence of the competition between two physical effects: the increase of the local Fermi level in the conduction band $k_F \propto \sqrt{N_c} \propto E_x^{3/4}$ and the increase of the distribution function shift $\delta k_x \propto E_x$. At the same time, the introduced deformation parameter η determines the relation between the numbers of spontaneous photons with x - and y -polarization, which follows from the expressions for the probability of spontaneous emission of an electron with given momentum direction (see Appendix of [37]).

A principle scheme of our experiment is shown in Fig. 2(a). THz pulses were generated in a LiNbO_3 crystal by the tilted-laser-pulse-technique using a femtosecond Ti:Sapphire laser (0.9 mJ, 70 fs, 600 Hz). The THz radiation was focused by a 2-inch off-axis parabolic mirror on a graphene sample at room temperature. The amplitude of the incident electric field reached up to 250 kV/cm (note that the electric field in the plane of the graphene sheet was smaller because of the substrate influence).

We used monolayer graphene on polyethylene terephthalate (PET) and glass substrates, and the results in both cases were similar. Note that a doping of graphene is of p-type and characteristic Fermi levels are -0.2 eV for glass and -0.35 eV for PET [42]. The forward emitted optical luminescence was collected by F1 lens ($D = 45$ mm and $\text{NA} = 1$) and focused by an objective lens F2 (Canon EF 50 mm F/1.4) on a CCD camera (SPEC-10:400BR Princeton Instruments, cooled down to -65°C). Camera exposure was set to 100 seconds. The emission spectrum was measured with a set of color filters.

In Fig. 2 (b) the experimentally measured dependencies of the spontaneous emission intensity on the THz field amplitude are presented for different spectral ranges. Slightly sharper dependencies for higher photon energies were observed. These data turned out to be key for finding $T(E_x)$ dependence discussed

¹ Eq. (7) is valid when the characteristic time of Landau-Zener transition $\delta t = \sqrt{\hbar/eE_x v_F}$ is less than the inversed momentum relaxation rate γ_a^{-1} [37]. Typically, this condition is fulfilled for THz fields stronger than 70-100 kV/cm ($\delta t = 8 - 10$ fs), which is also a threshold of intense pair production ($\sim 10^{12} - 10^{13}$ carriers per cm^2 for a sub-picosecond pulse).

above: we estimate the electronic temperature by comparing results of the simulations with the experimental results shown in Fig. 2(b). While the rest of numerical simulation results are weakly sensitive to temperature changes, the number of photons increase with the increase of the THz field cannot be correctly interpreted without considering temperature changes. The theoretical curves shown in Fig. 2(b) are obtained in the simulations with the linear fitting of electronic temperature increase $T(E_x) = 44 \text{ meV} + 1.1 \text{ meV} \cdot E_x [\text{kV/cm}]$ (numerical results presented in Fig. 3 and Fig. 4 are obtained with the same linear fitting). The intraband relaxation rate in these simulations was kept equal to 35 fs which is our best fit as will be shown further.

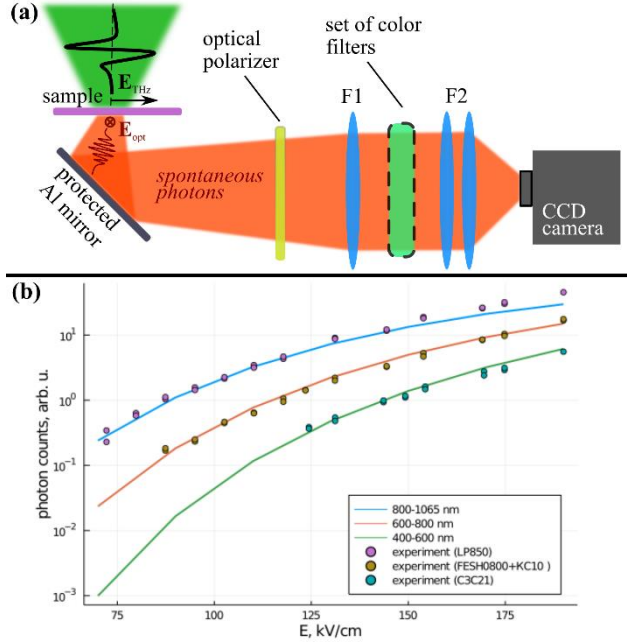


Fig. 2. (a) Principal scheme of the experimental setup. THz pulse is generated in a LiNbO₃ nonlinear crystal and incidents normally at the sample; optical emission transmitted through the substrate is detected in forward direction with different sets of color filters. (b) Graphene luminescence in different spectral ranges vs. THz field magnitude. Experimental data are represented by circles; corresponding spectral ranges are indicated in the inset. Solid color lines show the results of numerical modeling.

The second series of experiments was aimed to study the polarization features of optical radiation, the results are shown in Fig. 3. Despite the spontaneous character of emission, it occurred to be significantly polarized. Approximately 1.5 times more photons were polarized perpendicularly to the THz field and this ratio remained roughly constant in the whole range of THz field amplitudes 70–190 kV/cm.

Invariance of the ratio between two polarizations seemed to be the most difficult feature for the theoretical interpretation. However, it was also reproduced in the numerical modelling in the available range of THz magnitudes after including $T(E_{THz})$ dependence mentioned above. It occurs that the anisotropy of the distribution function is controlled by three main factors which effectively cancel out each other in the region of investigation. With increasing the THz pulse intensity, the anisotropy of the distribution function naturally grows due to a stronger disturbance by the electric field; on another side, the temperature is also growing and reduces anisotropy; finally, the local effective Fermi level is growing as well also decreasing the anisotropy. Note that the analytical estimation (9) doesn't take into account temperature increase, so it predicts the slowly growing dependence $\sim E_{THz}^{1/4}$.

In Fig. 3 the experimentally measured anisotropy is compared with the theoretical dependencies with several fixed relaxation rates γ_a : basing on this comparison we expect that, with available accuracy, the effective intraband relaxation time is 35 ± 5 fs. As seen from Fig. 3, the polarization of photons is rather

sensitive to this parameter. Also note that analytical estimation (9) predicts the relative deformation $\eta \approx 2.4$ which describes the distribution in Fig. 1 (c) with acceptable accuracy. However, high fluctuations in the experimentally measured number of photons didn't allow us to estimate this time with better precision. Anyway, the obtained time of the order of few tens of femtoseconds is in good agreement with other studies.

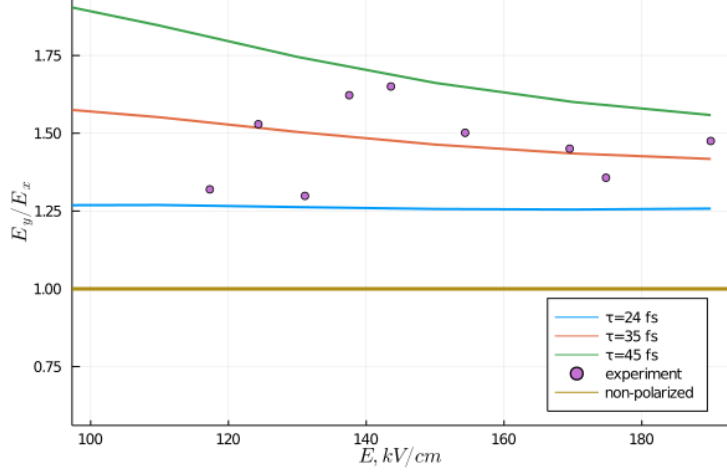


Fig. 3. Dependence of the emission anisotropy (the ratio between the number of photons with the polarization orthogonal and parallel to the THz electric field) on the THz field magnitude in the plane of graphene sheet. Circles – experimental data, color lines – numerical modeling results for different relaxation times γ_a^{-1} ; thick brown line corresponds to the isotropic case.

The optical emission spectra of graphene on the PET and glass substrates are shown in Fig. 4. They have quasi-thermal character, with effective temperatures of 0.185 eV and 0.22 eV for the glass and PET respectively (obtained by fitting with Planck distribution, not shown here). Numerical modelling demonstrated that this difference should be mostly attributed to the difference in the substrate dielectric properties which influence the electric field magnitude in the plane of graphene sheet (because of this the maximal field reduces to 190 kV/cm for PET and to 140 kV/cm for glass). Also, the Fermi levels are different, which was also taken into account. It is worth note that the electronic temperature estimated based on numerical simulations is slightly higher than the effective temperature of the emitted radiation. This confirms again that the radiation is of non-equilibrium nature despite being occurred to look like a thermal one.

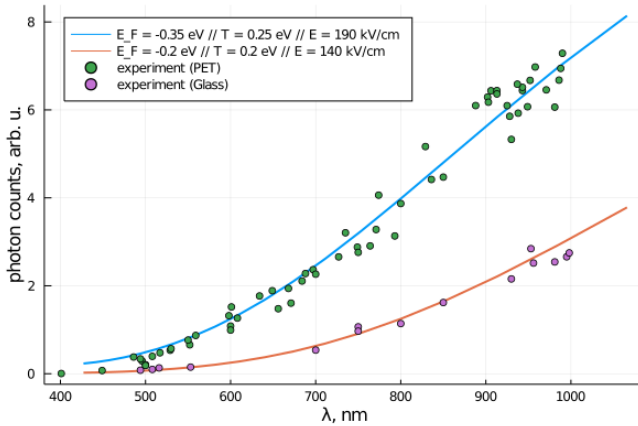


Fig. 4. The spectra of graphene luminescence induced by the action of THz pulse. Green and violet circles are experimental data for graphene on PET and on glass respectively. Blue and red lines represent numerical modeling with the parameters shown in the box (the intraband relaxation rate was

equal to 35 fs in both simulations); the THz field amplitudes are different because of the difference in the substrate permittivities.

To conclude, we measured the spontaneous optical emission of graphene with the strongly nonequilibrium carrier distribution excited by a single-cycle THz pulse. This broadband optical radiation has a quasithermal spectrum (in the range of 350-1050 nm) but occurs to be significantly polarized. Moreover, the ratio between the x and y -polarizations remains roughly constant with an increase of the incident THz field from 100 to 250 kV/cm. The analytical estimations and numerical modeling showed that the source of spontaneous emission are interband transitions of the excited electrons and that the presence of dominant polarization can be interpreted as a consequence of a strong deformation of the electronic distribution function. Also, the theory predicts weak dependence of the polarization anisotropy on the THz field strength which was confirmed with the available experimental accuracy. The measured dependencies of the luminescence intensities in different spectral ranges on the THz field magnitude allow us to roughly estimate the electronic temperature dependence on the THz field. The best fitting was achieved for $T(E_x) = 44 \text{ meV} + 1.1 \text{ meV} \cdot E_x [\text{kV/cm}]$ which can be used for further validation of microscopic heating models.

Finally, we would like to emphasize that the observation of a spontaneous optical emission after a sub-cycle THz excitation is a powerful experimental method for obtaining new data on ultrafast kinetics of nonequilibrium electrons in graphene, as well as in other materials. Being polarization-sensitive by its nature, this method gives a possibility to study an isotropization stage of a distribution function evolution.

Acknowledgements. The experimental part of the work was supported by RFBR grant #18-29-19091_mk. I.V.O. is grateful to the “Basis” foundation for personal support (grant # 19-1-4-61-1). The authors also thank prof. Alexey Belyanin for fruitful discussions. The simulations were performed on resources provided by the Joint Supercomputer Center of the Russian Academy of Sciences.

References

1. F. Bonaccorso, Z. Sun, T. Hasan, and A. Ferrari, *Nat. Photonics* 4, 611 (2010).
2. T. Gu, N. Petrone, J. F. McMillan, A. van der Zande, M. Yu, G.-Q. Lo, D.-L. Kwong, J. Hone, and C. W. Wong, *Nat. Photonics* 6, 554 (2012).
3. D. Sun, C. Divin, J. Rioux, J. E. Sipe, C. Berger, W. A. de Heer, P. N. First, and T. B. Norris, *Nano Lett.* 10, 1293 (2010).
4. Y. Q. An, F. Nelson, J. U. Lee, and A. C. Diebold, *Nano Lett.* 13, 2104 (2013).
5. H. K. Avetissian, A. K. Avetissian, G. F. Mkrtchian, and K. V. Sedrakian, *J. Nanophotonics* 6, 061702 (2012).
6. Jiang, T., Kravtsov, V., Tokman, M., Belyanin, A. & Raschke, M. B. Ultrafast coherent nonlinear nano optics and nanoimaging of graphene, *Nature Nanotechnology* 14 pp. 838-843 (2019)
7. H.A. Hafez, S. Kovalev, K.J. Tielrooij, M. Bonn, M. Gensch, D. Turchinovich, Terahertz nonlinear optics of graphene: from saturable absorption to high-harmonics generation, *Advanced Optical Materials* 8 (3), 1900771 (2020)

8. Hafez, H.A., Kovalev, S., Deinert, J.C. et al. Extremely efficient terahertz high-harmonic generation in graphene by hot Dirac fermions. *Nature* 561, 507–511 (2018)
9. M. Glazov and S. Ganichev, *Phys. Rep.* 535, 101 (2014)
10. X. Yao, M. Tokman, and A. Belyanin, *Phys. Rev. Lett.* 112, 055501 (2014)
11. T. J. Constant, S. M. Hornett, D. E. Chang, and E. Hendry, *Nat. Phys.* 12, 124 (2016).
12. J. C. König-Otto, M. Mittendorff, T. Winzer, F. Kadi, E. Malic, A. Knorr, C. Berger, W. A. de Heer, A. Pashkin, H. Schneider, M. Helm, and S. Winnerl, *Phys. Rev. Lett.* 117, 087401 (2016).
13. T. Li, L. Luo, M. Hupalo, J. Zhang, M. C. Tringides, J. Schmalian, and J. Wang, *Phys. Rev. Lett.* 108, 167401 (2012).
14. S. Wu, L. Mao, A. M. Jones, W. Yao, C. Zhang, and X. Xu, *Nano Lett.* 12, 2032 (2012)
15. C.B. Mendl, M. Polini, A. Lucas, Coherent terahertz radiation from a nonlinear oscillator of viscous electrons, *Applied Physics Letters* 118 (1), 013105 (2021)
16. D. A. Bandurin, D. Svintsov, I. Gayduchenko, S. G. Xu, A. Principi, M. Moskotin, I. Tretyakov, D. Yagodkin, S. Zhukov, T. Taniguchi, K. Watanabe, I. V. Grigorieva, M. Polini, G. N. Goltzman, A. K. Geim and G. Fedorov, Resonant terahertz detection using graphene plasmons, *Nature Communications* 9 (1), 1-8 (2018)
17. Mikhail Tokman, Yongrui Wang, Ivan Oladyshkin, A. Ryan Kutayah, and Alexey Belyanin. Laser-driven parametric instability and generation of entangled photon-plasmon states in graphene and topological insulators // *Phys. Rev. B* 93, 235422 (2016)
18. S. A. Mikhailov, Nonperturbative quasiclassical theory of graphene photoconductivity, *Physical Review B* 103 (24), 245406 (2021)
19. S. A. Mikhailov, Theory of the strongly nonlinear electrodynamic response of graphene: A hot electron model, *Physical Review B* 100 (11), 115416 (2019)
20. J. Cheng, N. Vermeulen, and J. Sipe, *Sci. Rep.* 7, 43843 (2017).
21. J. J. Dean and H. M. van Driel, *Appl. Phys. Lett.* 95, 261910 (2009).
22. J. J. Dean and H. M. van Driel, *Phys. Rev. B* 82, 125411 (2010).
23. Mikhail Tokman, Sergei B. Bodrov, Yuri A. Sergeev, Alexei I. Korytin, Ivan Oladyshkin, Yongrui Wang, Alexey Belyanin, and Andrei N. Stepanov. Second harmonic generation in graphene dressed by a strong terahertz field // *Phys. Rev. B* 99, 155411 (2019)
24. Yongrui Wang, Mikhail Tokman, and Alexey Belyanin. Second-order nonlinear optical response of graphene // *Phys. Rev. B* 94, 195442 (2016)
25. I. D. Tokman, Q. Chen, I. A. Shereshevsky, V. I. Pozdnyakova, I. Oladyshkin, M. Tokman, A. Belyanin, Inverse Faraday effect in graphene and Weyl semimetals, *Physical Review B* 101 (17), 174429 (2020)
26. Kim, M., Xu, S.G., Berdyugin, A.I. et al. Control of electron-electron interaction in graphene by proximity screening. *Nat Commun* 11, 2339 (2020).

27. S. Tani, F. Blanchard, and K. Tanaka, Phys. Rev. Lett. 109, 166603 (2012).

28. K. J. Tielrooij, J. C. W. Song, S. A. Jensen, A. Centeno, A. Pesquera, A. Zurutuza Elorza, M. Bonn, L. S. Levitov, and F. H. L. Koppens, Nat. Phys. 9, 248 (2013).

29. M. Mittendorff, T. Winzer, E. Malic, A. Knorr, C. Berger, W. A. de Heer, H. Schneider, M. Helm, and S. Winnerl, Nano Lett. 14, 1504 (2014).

30. D. Brida, A. Tomadin, C. Manzoni, Y. J. Kim, A. Lombardo, S. Milana, R. R. Nair, K. S. Novoselov, A. C. Ferrari, G. Cerullo, and M. Polini, Nat. Commun. 4, 1987 (2013).

31. T. Ploetzing, T. Winzer, E. Malic, D. Neumaier, A. Knorr, and H. Kurz, Nano Lett. 14, 5371 (2014).

32. T. Winzer, E. Malic, and A. Knorr, Phys. Rev. B 87, 165413 (2013).

33. T. Winzer, A. Knorr, and E. Malic, Nano Lett. 10, 4839 (2010).

34. E. Malic, T. Winzer, E. Bobkin, and A. Knorr, Phys. Rev. B 84, 205406 (2011)

35. E. Malic, T. Winzer, and A. Knorr, Appl. Phys. Lett. 101, 213110 (2012).

36. G. Kane, M. Lazzeriand, and F. Mauri, J. Phys. Condens. Matter. 27, 164205 (2015).

37. I.V. Oladyshkin, S.B. Bodrov, Yu.A. Sergeev, A.I.Korytin, M.D Tokman, A.N. Stepanov. Optical emission of graphene and electron-hole pair production induced by a strong terahertz field // Phys. Rev. B 96, 155401 (2017).

38. M. S. Foster and I. L. Aleiner, Phys. Rev. B 79, 085415 (2009)

39. Justin C. W. Song, Klaas J. Tielrooij, Frank H. L. Koppens, and Leonid S. Levitov. Photoexcited carrier dynamics and impact-excitation cascade in graphene // PHYSICAL REVIEW B 87, 155429 (2013), DOI: 10.1103/PhysRevB.87.155429

40. Brida, D. A. Tomadin, C. Manzoni, Y.J. Kim, A. Lombardo, S. Milana, R.R. Nair, K.S. Novoselov, A.C. Ferrari, G. Cerullo & M. Polini. Ultrafast collinear scattering and carrier multiplication in graphene. Nat. Commun. 4:1987 doi: 10.1038/ncomms2987 (2013)

41. Kotov, V. N., Uchoa, B., Pereira, V. M., Guinea, F. & Castro Neto, A. H. Electron-electron interactions in graphene: current status and perspectives. Rev. Mod. Phys. 84, 1067–1125 (2012)

42. P.R. Whelan, Q. Shen, B. Zhou et al., Fermi velocity renormalization in graphene probed by terahertz time-domain spectroscopy, 2D Materials 7, 035009 (2020)

43. C. H. Lui, K. F. Mak, J. Shan, and T. F. Heinz, Phys. Rev. Lett. 105, 127404 (2010)

44. H. Wang, J. H. Strait, P. A. George, S. Shivaraman, V. B. Shields, M. Chandrashekhar, J. Hwang, F. Rana, M. G. Spencer, C. S. Ruiz-Vargas, and J. Park, Appl. Phys. Lett. 96, 081917 (2010)

Supplementary Materials. Numerical modelling details

The density matrix equations were discretized on a 2D rectangular grid and numerically integrated by an operator splitting method [A1] in the following way. An advection term $\partial/\partial t - eE/\hbar\partial/\partial k_{x,y}$ has been integrated by means of the positivity flux conservative scheme [A2] from Vasilek.jl project [A3]. Rabi terms and damping terms were calculated by the simple Euler scheme. A written code has been tested against a number of simple problems with known results and has been shown to be stable and reasonably accurate. In all simulations a 300×100 box has been used corresponding to physical dimensions of $[-1.5, 1.5] \times [-1.5, 1.5]$ measured in $\text{eV}/\hbar\nu_F$. A time step was equal to $0.4\text{eV}^{-1} \cdot \hbar \approx 1.6$ fs and a total simulation time was equal to 7000 time steps or about 11.6 ps. Initially the Fermi distribution was set with a given Fermi energy of -0.35 eV for a PET substrate and -0.2 eV for a glass substrate. Other parameters were varied as indicated in the text.

The numbers of photons with x - and y -polarizations, spontaneously emitted per unit time due to the interband transition from given distribution $n_{c,v}(\mathbf{k})$, were calculated using the analytical relations given in the Appendix of [37]. Note that at room temperature the interband relaxation is caused mostly by electron-phonon interaction, so the spontaneous emission of photons is a process with a relatively low probability which modifies the distribution function insignificantly.

[A1] C.Z. Cheng and G. Knorr, *The integration of the Vlasov equation in configuration space*, *J. Comput. Phys.*, 22 (1976), pp. 330–351

[A2] Filbet, F., Sonnendrücker, E. & Bertrand, P. *Conservative Numerical Schemes for the Vlasov Equation*. *J. Comput. Phys.* 172, 166–187 (2001)

[A2] <https://github.com/korzhimanov/Vasilek.jl>